Title
MEASUREMENT OF Ku3+ DECAY PARAMETERS

Authors
Callahan, Andrew C.
Camerini, Ugo
Hantman, Ronald D.
et al.

Publication Date
1966-01-03

University of California

Ernest O. Lawrence Radiation Laboratory

MEASUREMENT OF $K^{+}_{\mu 3}$ DECAY PARAMETERS

Berkeley, California

DISCLAIMER

To be submitted to The Physical Review

UCRL-16593

UNIVERSITY OF CALIFORNIA

Lawrence Radiation Laboratory
Berkeley, California

AEC Contract No. W-7405-eng-48

MEASUREMENT OF $K^+_{\mu 3}$ DECAY PARAMETERS

Andrew C. Callahan, Ugo Camerini, Ronald D. Hantman, Robert H. March, David L. Murphree, George Gidal, George E. Kalmus, Wilson M. Powell, Carl L. Sandler, Robert T. Pu, Sergio Natali and Matteo Villani

January 3, 1966

MEASUREMENT OF $K^+_{\mu 3}$ DECAY PARAMETERS*

Andrew C. Callahan, Ugo Camerini, Ronald D. Hantman,
Robert H. March, and David L. Murphree†
Department of Physics
University of Wisconsin
Madison, Wisconsin

George Gidal, George E. Kalmus, Wilson M. Powell,
and Carl L. Sandler‡
Lawrence Radiation Laboratory
University of California
Berkeley, California

Robert T. Pu
Department of Physics
University of California
Riverside, California

and

Sergio Natali and Matteo Villani
Istituto di Fisica
Universita di Bari
Bari, Italy

January 3, 1966

ABSTRACT

K^+ mesons stopped in C_3F_8 in the LRL 30-inch heavy liquid bubble chamber were used in a study of the properties of the decay mode $K^+ \rightarrow \pi^0 + \mu^+ + \nu$. The properties studied were the μ^+ and π^0 energy spectra, μ^+ longitudinal polarization, μ^+ total polarization, and $K^+_{\mu 3}/K^+_{e 3}$ branching ratio. The data are consistent with the universal V-A theory, with time-reversal invariance and μ-e universality. Using the usual form-factor phenomenological expression for the strangeness-changing vector current, we obtain

$$\mathrm{Re}\ \xi = +0.34^{+0.42}_{-0.26}$$

$$\mathrm{Im}\ \xi = +0.69^{+0.85}_{-1.0}$$

$$\lambda_+ = 0.00 \pm 0.05$$

$$f_+ (K_{\mu 3})/f_+ (K_{e 3}) = 1.01 \pm .05 .$$

Im ξ should vanish by time-reversal invariance and $f_+(K_{\mu_3})/f_+(K_{e_3})$ should be unity if μ-e universality holds. With these assumptions we obtain Re $\xi = 0.41^{+0.27}_{-0.22}$.

I. INTRODUCTION

We have studied the properties of the $K^+_{\mu_3}$ decay mode ($K^+ \rightarrow \pi^0 + \mu^+ + \nu$) using data obtained from an exposure of the Berkeley 30-inch heavy liquid bubble chamber filled with C_3F_8 to a beam of stopping K^+ mesons. Preliminary results on parts of the work described have already been published.[1,2]

In all, five properties of the $K^+_{\mu_3}$ decay were studied experimentally:

1. The μ^+ energy spectrum in the range $42 < T_\mu < 94$ MeV (2648 events);
2. The μ^+ longitudinal polarization $38 < T_\mu < 95$ MeV (2950 events);
3. The K_{μ_3}/K_{e_3} branching ratio (636 K_{μ_3} events plus 873 K_{e_3} events);
4. The π^0 energy spectrum at fixed μ^+ energies $40 < T_\mu < 90$ MeV, $T_\pi < 110$ MeV (444 events);
5. The μ^+ total polarization $40 < T_\mu < 90$ MeV, $T_\pi < 110$ MeV (397 events).

Measurements 4 and 5 require completely reconstructed $K^+_{\mu_3}$ decays. Because the number of $K^+_{\mu_3}$ was rather small where the γ rays from the π^0 converted and the μ^+ stopped in the chamber, we performed experiments 1 and 2 using the two properties of the decay that can be measured without observing the π^0. In order to assure statistical independence, we deleted events used in 5 from the sample 2. The other experiments are already independent.

The data from these experiments may be used to establish the form of the interaction, which has previously been found to be consistent with vector;[3,4] we also find that our data are compatible with a pure vector interaction. With this established, the data may be used to determine detailed properties of the vector interaction. Experiment 3 provides a test of μ-e universality, and all five experiments may be used as tests of Time-Reversal Invariance in $K^+_{\mu_3}$ decay.

In the universal V-A theory of weak interactions, the matrix element for the $K^+_{\mu_3}$ decay may be written as[5]

$$M = \langle \pi | J_\nu | K \rangle \langle \nu | j_\nu | \mu \rangle,$$

where the lepton current is given by

$$j_\nu = \gamma_\mu (1 + \gamma_5),$$

and the strangeness-changing current J_ν can be expanded in terms of two form factors f_+ and f_- in the form

$$J_\nu = f_+ (q_K + q_\pi) + f_- (q_K - q_\pi),$$

where q_K and q_π are the K and π four-momenta, and f_+ and f_- are scalar functions of the four-momentum transfer squared $(q_K - q_\pi)^2$. Therefore, they depend only on the π^0 energy in the K^+ rest system. In most theoretical models these form factors (f_+ and f_-) should vary slowly with π^0 energy.[6,7]

All properties of the decay depend solely on f_+ and f_- and, apart from the absolute decay rate, all observables depend solely on the ratio $f_-/f_+ \equiv \xi$ (with f_+ and f_- assumed constant). Time-reversal invariance requires that ξ be real.[7]

Theoretical expressions for all the observables studied in this experiment are given in the Appendix; μ-e universality requires that the same matrix element describe $K^+_{e_3}$ decay ($K^+ \rightarrow \pi^0 + e^+ + \nu$) as $K^+_{\mu_3}$. As shown in the Appendix, all terms containing f_- contain the factor $(M_{lepton}/M_K)^2$; therefore, f_- is unmeasurable in $K^+_{e_3}$ decay and the hypothesis of μ-e universality resolves in practice to the statement that $f_+ (K_{e_3}) = f_+ (K_{\mu_3})$. This equality may be tested by using ξ obtained from $K^+_{\mu_3}$ decay to predict the $K^+_{\mu_3}/K^+_{e_3}$ relative branching ratio, and to compare it with the measured value of this ratio.

II. EXPERIMENTAL PROCEDURE

The beam, produced at 26° from an internal target in the Bevatron, had two stages of separation. The beam momentum was 800 MeV/c with a momentum bite of ±2%. The pion contamination at the second mass slit was

estimated at less than 1%. The beam was degraded by a copper sawtooth degrader at the bubble chamber entrance window, so that the K^+ stopping points were well spread out in the chamber. The stopping volume of the K^+ was approximately 30 cm long by 20 cm wide by 8 cm deep. This spreading of the K^+ decay points had the advantage of separating the origins for ease of scanning. The chamber was filled with C_3F_8, which has a density of 1.22 g cm^{-3} and a radiation length of 28 cm under operating conditions. A total of 240 000 pictures, containing about 3×10^6 stopping K^+ tracks, was taken.

Separate scans of the film provided the data for experiments 1, 2, 3, and 4; the same scan that was used for 4 was also used for 5. There was considerable overlap in the samples, which ranged in size from less than 20% of the film for experiment 3 to over 80% for 4 and 5.

In all cases the ionization of the K^+ had to be consistent with its being stopped, and the charged secondary from the K^+ decay also had to stop in the chamber and decay into an e^+. For measurements 4 and 5, both γ rays from the π^0 decay had to convert in the chamber to $e^\pm$ pairs. Figure 1 shows a K_{μ_3} decay where both γ rays from the π^0 convert.

Before energy and other cuts were made on the data, the total sample of separate events from all scans was about 12 000, of which about 10% had two conversion pairs.

The momentum of the μ^+ was obtained from range in all cases.

The principal sources of difficulty in this experiment were geometric biases and background from other K^+ decay modes.

The geometric biases originate from the fact that the range of the maximum-energy muon from K_{μ_3} decay is 46 cm, but the dimensions of the visible portion of our chamber are approximately 75 cm by 45 cm by 30 cm, the last dimension being parallel to the magnetic field. Therefore, the

probability that the μ^+ stops in the chamber is strongly energy dependent. In addition, for those events in which the $e^{\pm}$ pairs were observed, the effect of μ^+ detection on π^0 detection probability also had to be considered.

Most of the serious sources of background result from the short (1.4 mm) range of the μ^+ coming from a π^+ decay at rest; we determined experimentally, by examining π^+ endings from both K_τ's ($K^+ \rightarrow \pi^+ + \pi^+ + \pi^-$) and $K^+_{\pi_2}$'s ($K^+ \rightarrow \pi^+ + \pi^0$), that from 12 to 30% of the time a μ^+ track cannot be distinguished from its parent π^+ track and, thus, a stopping π^+ resembles a stopping μ^+. The exact ratio varies with film quality and stringency of scanning instructions.

The short μ^+ introduces background from two modes

$$K_{\pi_2}: \; K^+ \rightarrow \pi^+ + \pi^0$$

$$K_{\tau'}: \; K^+ \rightarrow \pi^+ + \pi^0 + \pi^0 .$$

The first mode produces a π^+ of unique range, which corresponds to the range of a μ^+ of kinetic energy 100 MeV. The π^+'s from the second mode simulate μ^+'s of kinetic energy < 48 MeV. It is largely these two backgrounds that dictate the limits on muon energies used in each experiment.

Other minor sources of background that are common to all the experiments are, first, the $K^+_{\mu_3}$ decays where the K^+ decays in flight but is close enough to the end of its range so that it is not possible to tell that it is in flight from its ionization. In our film this restricted the K^+ momentum to < 200 MeV/c. Only about 3% of all K's below this momentum will decay in flight. Second, K_{π_2} and $K_{\tau'}$ decays (in which the π^+ decays in flight to a μ^+), can be mistaken for K_{μ_3}'s if the π-μ angle in the laboratory system is small.

How we dealt with the above biases and problems associated with individual experiments is described below:

1. μ^+ Energy Spectrum

In this study 2648 events were identified solely by means of a stopping μ^+. The criteria imposed in scanning were slightly different at Berkeley[8] and Wisconsin;[9] thus the samples from these two Laboratories were analyzed separately and the likelihood functions combined. They proved completely consistent. The criteria used were:

(a) Events with $42 < T_\mu < 94$ MeV were accepted. This cut eliminated the region in which background from K_τ and K_{π_2} is high. The endpoint of of the τ' spectrum corresponds to $T_\mu = 48$ MeV; the region from 42 to 48 contains a negligible number of τ' events. The π^+'s from K_{π_2} have the same range as 100 MeV/c μ^+'s.

(b) Tracks with dip angles greater than 60° were discarded, because they are difficult to identify and measure.

(c) No tracks with a visible $\pi \rightarrow \mu \rightarrow e$ chain at the end were accepted. This eliminated the few remaining K_τ, K_{π_2} background events and backgrounds from these modes by K^+ decay in flight.

(d) The μ^+ must stop inside a fiducial volume (slightly smaller than the visible portion of the chamber). This criterion was adopted to permit an accurate estimate of the detection efficiency.

(e) No events with visible "kinks" in the decay secondary were accepted. This criterion served to reduce the principal remaining source of background—K_{π_2} events with a π-μ decay in flight.

Criterion (e) was applied slightly differently at the two Laboratories. At Wisconsin, the angular distribution of kinks in events rejected by the scanners under criterion (d) was determined; they found that the average space angle below which a kink was not observed was 12°. The final data sample was corrected to remove the background of K_{π_2} events with kinks

less than 12°, a correction of 9%. At Berkeley, tracks with "muon" ranges of 20 to 28 cm, which originate from events in which the $\pi \rightarrow \mu$ center-of-mass decay angle is large and thus the laboratory decay angle is always 8°, or greater, were carefully examined on a projector that permitted superposition of tracks from different views; the correction for the remaining background of events with ranges less than 20 cm or which escape the examination is 4.6%.

The next most serious background--about 3%--was due to radiative $K_{\mu 2}$ decay. The contamination from all other backgrounds, including $K_{\mu 2}$ decays in flight and high energy τ' decays, were smaller than this figure, though in a small region of the spectrum corrections were necessary. Corrections were also made for the slight distortion of the spectrum due to the decay in flight of about 3% of the K^+'s in the sample.

By means of a second scan, the data were checked for energy-dependent scanning biases. No significant bias was found. Scanning efficiency was 85% or greater in all regions of the spectrum at both Laboratories.

The final data samples were corrected for muon-escape bias by means of Monte Carlo programs essentially the same as those described in Sec. II. B. 3, with the result shown in Fig. 2 (curve B). The results of two programs at Wisconsin and one at Berkeley, with somewhat different methods used for generating the μ^+ tracks, were compared and found to agree to within about 2% at all energies. In the likelihood-function computation, the Monte Carlo geometrical correction was used to correct the theoretical muon spectrum [Eq. (A6) in the Appendix].

2. μ^+ Longitudinal Polarization

All experimental details of this aspect of the experiment have been described previously by Gidal, et al.[2]

The number of events remaining after all cuts was 2950 in the range

$38 < T_\mu < 95$ MeV. The only change from results reported in Reference 2 was the deletion of 38 events used in the total polarization analysis, in order to maintain statistical independence of the results of the separate measurements. On the basis of scanning efficiency and differences in selection criteria, an overlap of about 50 events would have been expected.

3. $K_{\mu 3}/K_{e 3}$ Branching Ratio

In this portion of the experiment, a selected sample of 50 rolls (about 20% of the film) was scanned by restrictive procedures designed to reduce systematic errors due to geometric biases and backgrounds. These procedures were as follows:

(a) Information from charged secondaries only was used. This restriction eliminated the need to estimate absolute detection probabilities of γ rays by pair production.

(b) A restricted fiducial volume at the beam-entry end of the chamber was carefully scanned twice for stopping charged secondaries. This resulted in a high scanning efficiency; comparison of events found on the two scans indicated each was more than 90% efficient, for an estimated efficiency greater than 99% on the double scan.

(c) Only tracks within 45° (both dip and azimuth) of the chamber's long axis were retained in the sample. Together with (b), this procedure increased the average path length available to charged secondaries, reducing the energy dependence of the detection efficiency to that corresponding to the upper curve in Fig. 2(A).

(d) Muon secondaries were required to stop in a well-defined fiducial volume slightly smaller than the chamber. Secondaries with ranges less than 1 cm were discarded, as scanning may be unreliable for such short tracks.

(e) Any track that went through a maximum radius from the K-decay origin before stopping or leaving the chamber was considered an electron. Under our conditions about 70% of all electrons from K_{e_3} decay will do this, and no heavier particle can.

(f) K^+ decays in flight were eliminated by a gap count in the last 3 cm of track. This criterion was calibrated against τ decays, where decays in flight are kinematically obvious. The calibration indicated that 3.2% of events that pass this test as though they were at rest were actually decays in flight.

(g) A simultaneous count of τ decays in the decay fiducial volume served to calibrate absolute rates.

The detection probability for the K_{μ_3} events was calculated as follows: A Monte Carlo computer program generated randomly oriented events of specified μ^+ range from a sample of actual K^+ decay vertices within the decay fiducial volume. The stopping position of the μ^+ was obtained, with curvature and multiple scattering taken into account, and tested for presence inside the larger fiducial volume described in procedure (d). This computation was repeated for 2, 4, 6, $\cdots$, 46-cm tracks; the number of actual events was divided by secondary range into 2-cm histogram bins centered on these values, and corrected accordingly.

A similar program determined the electron-detection efficiency, with additional terms to deal with the (a) effects of energy loss and angular deviation due to radiation, (from the Bethe-Heitler formula), and (b) loss of positrons through annihilation (with the Dirac formula used for the cross section). Since we could not measure electron energies with precision, we computed a weighted average detection efficiency of 68.1% by assuming a pure vector spectrum; a

pure scalar spectrum would reduce this by about 10%. Both detection-efficiency programs were compared with others written elsewhere with very good agreement. We estimated the reliability of this calculation as 4%, and folded the corresponding error into the result.

The major difficulty in the K_{μ_3} rate determination came from backgrounds. Eliminating events with secondary ranges from 29 to 33 cm, which are primarily K_{π_2}, left a sample of 1082 events, of which we estimated 636 were K_{μ_3}. Of the remaining background, about 373 events were $K_{\tau'}$, with 73 from various minor sources (radiative K_{μ_2}, and $K_{\pi 2}$ followed by $\pi \rightarrow \mu + \nu$ in flight provided the greatest share). The $K_{\tau'}$ correction was obtained in two separate ways. Our final number was computed directly from the rate and π^+ spectrum given by Bisi et al.,[11] and no attempt was made to identify $K_{\tau'}$ events by the $\pi^+ \rightarrow \mu^+ \rightarrow e^+$ decay signature. An estimate based on counting events with this signature and estimating the number in which the μ is missed gives essentially the same result—276 $K_{\tau'}$ identified plus an estimated 106 missed for a total of 382—but we prefer not to rely on our estimate of the μ-stub-recognition efficiency.

With additional corrections (of the order of 1 to 3%) for events lost in the K_{π_2} region, events with μ tracks less than 1 cm, $K^+_{\mu 3}$ decays in flight, and scanning efficiency, we obtained our final sample, which we then corrected for detection efficiency.

For the K_{e_3} mode, we had a sample of 873 events. These were nearly free from background, the principal source being $K_{\tau'}$ decays in which both the π^+ and the μ^+ from its decay were missed. We estimated this background at about 1%. The weak point in the rate determination was clearly the detection-efficiency calculation, but unless there was a major scalar component in the decay this should have been reliable to about 3%.[3]

To obtain absolute rates, the 9983 K_{τ} mode events (no angular cutoff) found in the decay fiducial volume were used as a standard.

4. π^0 Spectrum at Constant μ^+ Energy

For this experiment about 150 000 pictures were scanned for K_{μ_3} events where the μ^+ stopped in the chamber and two $e^{\pm}$ pairs pointed back to the K^+ decay origin. Any event where there was a recognizable π-μ-e chain at the end of the charged secondary was rejected, as were events where the range of the charged secondary was less than 5 mm in space. Only events where both γ rays converted into $e^{\pm}$ pairs were accepted; when the γ's produced Compton electrons, they were rejected. The $e^{\pm}$ pairs had to point to the K^+ origin in all three stereo views.

The scan produced about 1200 candidates. These were measured and constrained to the K_{μ_3} hypothesis by means of a two-vertex simultaneous fit. The μ energy was obtained from range, and the γ-ray energy was found from the sum of the electron energies in each pair. The electron momenta were obtained by the Behr-Mittner method.[12] Although the errors on the electron momenta were large ($\gtrsim 35\%$), the error on the π^0 momentum was quite small, after constraint to a π^0 mass. We checked this figure experimentally by measuring a sample of K_{π_2} decays in which the π^0 had a unique momentum of 205.2 MeV/c. Figure 3 shows the π^0 momentum distribution from a sample of K_{π_2}, the two $e^{\pm}$ pairs being constrained to a π^0 mass. To check the reliability of the kinematic fitting programs, we measured some events both at Berkeley and at Wisconsin, and obtained the same results.

After measurement, events were rejected if the $e^{\pm}$ pairs did not point to the origin even though they appeared to on the scan table. After constraint, about 750 events fitted the K_{μ_3} hypothesis satisfactorily.

In spite of the constraint, it is possible for $K_{\tau'}$ and K_{π_2} events to fit the K_{μ_3} hypothesis. This was found to be true for $K_{\tau'}$ events by constraining a set of $K_{\tau'}$ events in which three or four γ rays converted, as K_{μ_3}'s; the input to the constraint program was the charged secondary and two of the γ rays. Indeed, events in which γ's not originating from the same π^0 are matched fit K_{μ_3} much of the time, but they can not fit the $K_{\tau'}$ mode, which has a much smaller Q-value and is therefore a tighter constraint.

In order to eliminate both these backgrounds, we made energy cuts on the μ^+. Using the shape of the π^+ spectrum from $K_{\tau'}$ decay,[13] we calculated that (after kinematic fitting) a lower cut of $T_\mu = 40$ MeV would give us a background from $K_{\tau'}$ of <1%. An upper cut of $T_\mu = 90$ MeV ensured that no normal K_{π_2} decays were in our sample. Events with $T_\mu > 110$ MeV could also be used, but there were too few of these to be of significance in our analysis.

The one other significant background in these data is that due to K_{π_2} decays in which the π^+ decays in flight to a μ^+ and the π-μ decay angle is too small to be seen. In 4.1% of the K_{π_2}, the π decays in flight, and in approximately half of these the π-μ angle is too small to be seen. A property of this decay that can be utilized, however, is that the π^0 and the π^+ in a K_{π_2} are collinear. After the γ rays are constrained to a π^0 mass, the π^0 direction (in both K_{π_2} and in K_{μ_3}) is known to within about 5°, so that a cut in the angle between the π^0 and charged secondary would eliminate this background (unlike experiments 1, 2, and 3, in which corrections for this were made).

Lines of constant π^0-μ^+ angle near 180°, when plotted on the T_π-versus-T_μ Dalitz plot, are very nearly lines of constant T_{π^0} in the energy region of this experiment. A cut based on π^0 energy rather than collinearity simplifies the data analysis. Using a sample of 250 events obtained by falsifying the π range on known K_{π_2} events and fitting them to K_{μ_3}, we

determined that a simple cut on the π^0 energy at $T_{\pi 0} = 110$ MeV would eliminate all but 8% of the K_{π_2}, π-μ decay in flight background, and reduce this to a total background of less than 1% (which was not significant with our statistics).

About 50% of the film was rescanned to determine scanning efficiency. A comparison of the μ^+ energy spectra from the two scans indicated a small scanning bias against higher energy μ^+. (This was only for the events with two conversion pairs.) We found no detectable bias in the π^0 energy spectrum; this lack was not surprising because the configuration and appearance of the $e^{\pm}$ pairs in the bubble chamber are only weakly energy dependent.

Therefore, we decided not to use the Dalitz-plot density in our final analysis, but instead used a maximum-likelihood fit to the π^0 spectrum at each μ^+ energy. This has the effect of taking out the μ dependence in the Dalitz plot information while retaining the π-μ correlation information.

After all cuts were made, 444 events remained in the region $40 < T_\mu < 90$ MeV and $T_{\pi 0} < 110$ MeV.

The finite size of the chamber introduced a correlation in the detection probability of the π^0 and the μ^+; many events with high-energy μ^+'s that stop in the chamber stop near the edge of the chamber. To determine the magnitude of this correlation, we used a Monte Carlo program that generated μ^+ events as described in Sec. II. B. 3. If the μ^+ stopped in the chamber, a π^0 of specified energy, at the appropriate angle to the μ^+ but otherwise random in direction, was generated at the decay origin. A random decay angle in the π^0 center of mass was chosen and the γ-ray conversion probability was then computed from the available path length. Independent programs at Wisconsin and Berkeley again gave compatible results. The effect of this correlation was to reduce the detection probability of a high-energy π^0 about

15%, with respect to that for a low-energy π^0 at high μ^+ energies. The results were expressed as a polynomial in T_μ and T_π; an example of the dependence of the detection probability on T_μ at T_π = 90 MeV is shown in curve C of Fig. 2.

5. Total Polarization of the μ^+

One additional cut was applied to the 444 events obtained in Sec. II. 4. This cut was one that was found to be both necessary and adequate in the longitudinal polarization data where sufficient statistics were available to measure the polarization as a function of position in the chamber.[2] It was found that there was a scanning bias against detecting K_{μ_3} events when the μ^+ stopped close to the top or bottom windows and the decay electron left the chamber. These events preferentially have an angle between the μ^+ track and e^+ track of $<90°$, which causes bias in the longitudinal component of the total polarization. Therefore, we cut all events where the μ^+ stopped within 4 cm of either top or bottom windows.

For this analysis the direction of the decay electron from the μ^+ was measured. This direction, together with the completely reconstructed K_{μ_3} decay and its orientation with respect to the bubble chamber magnetic field, was all that was needed for the analysis.

Scanning and geometric biases in the detection of the μ^+ do not affect these results, because in the data analysis the theoretical polarization was calculated separately for each event, i.e., no weighting procedure was used.

III. RESULTS AND ANALYSIS

The expressions used to form the likelihood functions in this section are given in the Appendix.

1. μ^+ Energy Spectrum (2648 events)

The experimental μ^+ spectrum, after background was subtracted and corrections were made for detection probability, is shown in Fig. 4.

Because the μ^+ energy spectrum is not very sensitive to the energy dependence of ξ, we assumed that both Re ξ and Im ξ were energy independent, and formed a two-parameter likelihood function (Appendix, Sec. A) in the two variables. Since the μ^+ energy region and the treatment of the data at the two laboratories were not identical, only the combined likelihood functions were used to determine ξ.

Figure 5 shows contours of equal likelihood on a map of Re ξ and $|\text{Im } \xi|$. One useful property of a two-parameter likelihood function is that to the approximation that it is the product of two Gaussian distributions, the confidence level is numerically equal to the value of the function, normalized to the peak value as unity. (This equality holds for the two-parameter case only.) Thus, the contours on all the two-parameter likelihood plots shown may be used for estimation of confidence levels.

For the μ^+ spectrum data we obtain, by reading off the numbers at the $e^{-1/2}$ contour;

$$\text{Re } \xi = 0.0^{+1.1}_{-0.9}$$

$$|\text{Im } \xi| = 0.0 \pm 1.0 \ .$$

2. μ^+ Longitudinal Polarization (2950 events)

We reanalyzed the results obtained on the same film scanned by Gidal et al.,[2] using the two-parameter likelihood function given in the Appendix (Sec. B) and deleting from the sample of reference 2 those 38 events that appear in the sample for the total polarization. Figure 6 shows the contours of constant likelihood of this function.

From the μ^+ longitudinal polarization we obtain

$$\text{Re } \xi = -0.7^{+0.9}_{-3.3}$$

$$|\text{Im } \xi| = 0.5^{+1.4}_{-0.5} ,$$

where again the errors quoted are to the $e^{-1/2}$ contour. As may be seen from the contours in Fig. 7, errors assigned this way are not very meaningful. However, the region just above Re $\xi = 0$ is a region of high sensitivity and thus this measurement does contribute significantly to our final result.

3. K_{μ_3}/K_{e_3} Branching Ratio (636 K_{μ_3} and 873 K_{e_3} events)

We obtain directly

$$R = (K^+_{\mu_3})/(K^+_{e_3}) = (0.703 \pm 0.056).$$

Assuming a K_τ mode branching ratio of 5.46%,[14] we obtain the absolute rates

$$(K^+_{\mu_3})/(\text{all } K^+) = (2.77 \pm 0.19)\%$$
$$(K^+_{e_3})/(\text{all } K^+) = (3.94 \pm 0.21)\%.$$

The errors include allowance for uncertainty in detection efficiency (2% in K_{μ_3}, 3% in K_{e_3}), and the absolute rates also allow for uncertainty in the τ rate.

Equation (A12) gives R as a function of ξ, with μ-e universality assumed. Solving this equation for a complex ξ defines a circle in the ξ plane with its center at -3.29 on the real axis, the radius squared being given by

$$|\xi + 3.29|^2 = 10.83 + 51.87\ (R - 0.648).$$

From our value of R, we obtain

$$|\xi + 3.29|^2 = 13.63 \pm 2.90.$$

The intersections with the real ξ axis are

$$\text{Re } \xi = +0.40 \pm 0.40 \text{ and } -6.98 \pm 0.40.$$

We obtained a test of μ-e universality by comparing this circle with the values of Re ξ and Im ξ predicted from all our other measurement. A spectrum-dependent measurement of the $K^+_{\mu_3}$ branching ratio was obtained by integrating the μ^+ energy spectrum found at Berkeley and normalizing to K_τ decays.[8] The result was $(2.93 \pm 0.23)\%$.

4. π^0 Spectrum at Fixed μ^+ Energies (444 events)

Figure 7 is a grid containing numbers that summarize the points on a Dalitz plot of the 444 events. The density of events predicted by V-A theory for $\xi = +0 + 0i$ (close to our final value) is also shown on the plot. The theoretical values there have been corrected for geometric detection efficiency in different kinematic regions, as described in Sec. II. 4.

As stated in Sec. II. 4, due to a possible μ^+ scanning bias in these events we decided to perform the analysis in a slightly different way. Instead of a straightforward application of the maximum-likelihood method on the Dalitz plot, we compared the expected π^0 spectrum at the known μ^+ energy with the data, event by event. The π^0 spectra were thus automatically weighted by the number of actual experimental events in each interval, but the likelihood function was independent of the muon spectrum itself.

It should be emphasized that the above technique is not the same as fitting the π^0 energy spectrum, as the π-μ correlation information is retained; in each case the π^0 spectrum has been compared to that expected for the appropriate μ^+ energy.

Little information is lost when this method is used because the π^0 energy distribution is more sensitive to the value of ξ than is the μ^+ energy distribution.

Formulae pertaining to the analysis as well as a more detailed description of the detection-efficiency program are given in Appendix A.

Figure 8 shows contours of constant likelihood on a plot of Re ξ versus $|\text{Im } \xi|$ for the above data. These contours assume constant form

factors. The data very nearly contain a "circle ambiguity." Thus, if Im ξ is 0 we have a sensitive measurement of Re ξ, but the data give little information on $|\text{Im } \xi|$.

The best value of Re ξ for Im $\xi = 0$ is Re $\xi = +0.72 \pm 0.37$.

The second solution, only a sixth as likely as the first, is Re $\xi = -4.83 \pm 0.25$.

All other measurements reported in this paper suggest large betting odds against this second solution.

The energy dependence of f_+ and f_- was tested by means of the first-order expansion

$$f_\pm = f_\pm^0 \left[1 + \lambda_\pm \frac{(q_K - q_\pi)^2}{m_\pi^2} \right] , \qquad (1)$$

where $f_\pm^0$ is the value of f_+ or f_- at $T_{\pi 0} = 0$. Since $q_K - q_\pi$ depends solely on the π^0 energy, only the π^0 spectrum data are useful for this test.

We recomputed the maximum-likelihood function with λ_- equal to zero, varying λ_+, and then with λ_+ equal to zero varying λ_-. A complete 4-parameter analysis was not justified at our level of statistical accuracy.

The values obtained from this analysis are given in Table I, which also shows the dependence of Re ξ on $\lambda_\pm$. It is clear that λ_- remains essentially undetermined.

Figure 9 shows the likelihood function for λ_+ with λ_- assumed to be zero. From this function we obtain

$$\lambda_+ = 0.00 \pm 0.05.$$

When this value of λ_+ and its errors are folded into the value we obtained above for Re $\xi = 0.72 \pm 0.37$ (Im $\xi = 0$, and $\lambda_\pm = 0$), we obtain

$$\text{Re } \xi = +0.72 \pm 0.80.$$

Recent measurements of λ_+ in K_{e_3} decay give a mean value of $\lambda_+ = 0.014 \pm 0.020$.[15] So, with μ-e universality assumed (see Sec. IV. for our results on this), the error quoted above for Re ξ is rather conservative. There are general theoretical considerations that also make it unlikely that the magnitude of λ_+ exceeds 0.03.

Figure 10 shows the experimental π^0 spectrum from the 444 events. The curves are the theoretical curves for scalar, vector ($\xi = 0 + 0i$), and tensor interactions. The theoretical curves have had the experimental μ^+ spectrum from the 444 events in the range $40 < T_\mu < 90$ MeV folded in. The probability of the distribution giving either pure scalar or tensor is <1%, whereas the vector ($\xi = 0$) gives better than 50% probability.

5. Total Polarization of the μ^+ (397 events)

It has been shown that the muon in K_{μ_3} decay is always completely polarized along some direction.[16] This follows from the assumptions that the leptons are produced at a point, the π and K spins are zero, and that the neutrino has a definite helicity. The direction of this polarization is a function of $\underset{\sim}{p}_\pi$, $\underset{\sim}{p}_\mu$, Re ξ, and Im ξ; this function is given in Eqs. (A7) and (A8).

Because the expression for the polarization involves a term in Im ξ [unlike all the others which contain only $(\text{Im } \xi)^2$], this measurement is sensitive to the sign of Im ξ. Note that the polarization is the only measurement that has this property, which is due to the time-reversal-violating component of the polarization, normal to the K decay plane.

The parity-nonconserving μ^+-e^+ decay was used to analyze the μ^+ polarization.

Because this experiment was done in a magnetic field, the only conserved component of the μ polarization was the one parallel to the magnetic field. To check that this component was conserved, we used K_{μ_2} decays, as

described in Ref. 2. The 16-kG field in this experiment should be adequate to prevent depolarization.

The expression used to form a two-parameter likelihood function (Re ξ and Im ξ) is given in Eq. (A11).

Figure 11 shows the $e^{-1/2}$, e^{-1}, and e^{-2} contours on the two-parameter likelihood plot. From this we obtain

$$\text{Re } \xi = -1.4 \pm 1.8$$

$$\text{Im } \xi = +1.6 \pm 1.3,$$

where the errors are quoted at the $e^{-1/2}$ (61%) level.

IV. DISCUSSION

1. Experimental

The vector nature of the interaction has been checked in three independent ways:

1. By fitting the μ^+ spectrum from measurement 1 with its final best values of Re ξ = 0 and Im ξ = 0, we obtained a χ^2 of 30 for 27 degrees of freedom (30%) for vector, a very satisfactory fit.[9] Tensor and scalar have <1% chance of fitting.
2. By fitting the π^0 spectrum from measurement 4, we obtained a χ^2 of 3 for 5 degrees of freedom (70%) for vector (ξ = 0). Tensor and scalar again have a probability of <1%.
3. The fact that measurements 1, 2, 4, and 5 all give consistent values of Re ξ and Im ξ is also a check on the nature of the interaction.

With the exception of the K_{e_3}/K_{μ_3} branching ratio, all our analysis was done with the maximum-likelihood method. Figures 5, 6, 8, and 11 show the results obtained by this type of analysis from the μ^+ spectrum, the μ^+ longitudinal polarization, the π^0 spectrum at fixed μ^+ energies, and the μ^+

total polarization, respectively. These measurements are independent in our experiment (events used for μ^+ total polarization were deleted from the sample used for longitudinal polarization). In these likelihood plots, constant form factors were assumed.

In order to obtain our best value of Re ξ and Im ξ, we multiplied the values on the four likelihood plots and plotted the results on Fig. 12. Note that the area enclosed in the $e^{-1/2}$ contour in the combined likelihood plot is quite probable in all the individual likelihood plots. The confidence levels for our best solution range from 0.53 → 0.80 in the individual measurements.

From this plot, assuming energy-independent form factors, we obtain:

$$\text{Re } \xi = 0.34^{+0.42}_{-0.26}$$

$$\text{Im } \xi = 0.69^{+0.85}_{-1.0} ,$$

which is consistent with time-reversal invariance, i.e., Im $\xi = 0$. If we assume Im $\xi = 0$, then Re ξ is better determined as $0.43^{+.37}_{-.27}$.

By direct test in the experiment in which we measured the π^0 spectrum at fixed μ^+ energies, we obtained a value for the energy dependence of f_+, defined in Eq. (1) $\lambda_+ = 0.00 \pm 0.05$. This value is consistent with the λ_+ value of -0.05 ± 0.07 obtained by Jensen et al.[17] for $K^+_{\mu_3}$, and also with the value of 0.014 ± 0.020, the world average for λ_+ from $K^+_{e_3}$ data. Despite the rapid variation of our best value of Re ξ with λ_+, we feel that at our level of statistical accuracy an analysis with constant form factors is justified. Allowing for the uncertainty in λ_+ would slightly increase the statistical errors quoted above.

We have insufficient data to determine a value for the energy dependence of f_-. In most theoretical models [see Ref. 7 for a summary], this value should be of the same order of magnitude as that for f_+.

Using Eq. (A12) and our value of ξ, one can predict the K_{μ_3}/K_{e_3} branching ratio to be $R = 0.693 \pm 0.037$. Compare this with the value we determined directly for $R = 0.703 \pm 0.056$. The comparison may be stated as

$$f_+(K_{\mu_3})/f_+(K_{e_3}) = 1.01 \pm 0.05,$$

which is a test of μ-e universality. Because of the form of our final likelihood function, with its slowest variation nearly along a curve of constant branching ratio, this conclusion is independent of the validity of time-reversal invariance.

If we assume exact universality, we may use the branching-ratio measurement to improve the value of Re ξ, obtaining

$$\text{Re } \xi = +0.41^{+0.27}_{-0.22}.$$

As a check of internal consistency, our final values of Re ξ and Im ξ give a χ^2 of 3.65 for 4 degrees of freedom when compared with the results of the five individual determinations.

Table II summarizes other recent determinations of Re ξ and Im ξ.

2. Theoretical

In the simplest theoretical model, that is with no K-π interaction and K-π mass degeneracy, ξ vanishes identically. In models that take into account the K-π interaction (summarized in Ref. 7), one expects that $|\xi|$ will be $\lesssim 1$, and that λ_+ and λ_- will decrease by $(M_\pi/M_K)^2$. In general, an intermediate vector boson, or a p-wave K-π interaction, give $(M_\pi/M_K)^2\, \xi \simeq -\lambda_+ \simeq \lambda_-$. If a single vector state, or a mixture of states with known relative coupling strength dominates, a numerical prediction can be made. For example, dominance by the $K^*_{1/2}$ (890 MeV) gives $\xi = -0.29$ and $\lambda_+ = -\lambda_- = 0.02$. If an s-wave K-$\pi$ interaction dominates, a similar relation holds between the magnitudes of ξ and the λ's, with ξ expected to be positive.

Our data are not precise enough to distinguish with any confidence among these models.

Most of the theories advanced to account for the apparent violation of CP invariance[18] in K_2^0 decay predict no violation of T invariance in $K_{\mu 3}^+$ decay. One exception is Cabibbo's[19] theory in which an effect would be expected, with Re $\xi = 0$ and Im $\xi \neq 0$. The magnitude of Im ξ in this theory, however, could well be too small to have been seen in our experiment.[20]

ACKNOWLEDGMENTS

The authors thank the staffs of the Bevatron and the 30-inch heavy liquid bubble chamber for their indispensible assistance with this experiment. We thank also Dr. Robert W. Birge and Dr. Robert P. Ely, Jr., for their work on the beam and for many helpful discussions. Dr. Adam Bincer, Dr. Nicola Cabibbo, Dr. Alexander T. Maksymowicz, Dr. Robert G. Sachs, and Dr. Bunji Sakita contributed illuminating discussions on the theoretical aspects of the problem. Finally, we acknowledge the assistance of Edward Strasbourger in much of the computer programming.

APPENDICES

We present here the theoretical expressions of the various quantities from which we form maximum-likelihood functions to obtain the best values of ξ from our experimental data. Where the expression is unnormalized, $\approx$ is used in place of $=$. References from which these expressions were taken are given. We have used complex form factors and made some minor changes in notation.

Notation

$E_{\mu, \nu, \pi}$	total energy of μ, ν, or π
$\underset{\sim}{p}_{\mu, \nu, \pi}$	momentum vector of μ, ν, or π
$\underset{\sim}{P}_{\mu}$	polarization vector of μ
P_{μ}^{ℓ}, $P_{\mu}^{\perp}$, P_{μ}^{t}	components of $\underset{\sim}{P}_{\mu}$ in the direction of the μ (longitudinal polarization), the normal to the decay plane, and the transverse direction in the decay plane, respectively.
$E'_{\mu, \pi}$	$E_{\mu, \pi}^{\text{Max}} - E_{\mu, \pi}$, where $E_{\mu, \pi}^{\text{Max}}$ is the maximum possible energy of the particle from K^+ decay at rest; i.e., $E_{\mu, \pi}^{\text{Max}} = \frac{1}{2 M_K}\left[M_K^2 + m_{\mu, \pi}^2 - m_{\pi, \mu}^2\right]$.
M_K, $m_{\mu, \pi}$	masses
f_+, f_-	form factors
ξ	ratio f_-/f_+

A. Dalitz Plot Density

The universal V-A theory gives the Dalitz-plot density function as[5]

$$\rho(\xi, E_{\mu}, E_{\pi}) \approx \{A(E_{\mu}, E_{\pi}) + B(E_{\mu}, E_{\pi}) \operatorname{Re} \xi + C(E_{\pi}) |\xi|^2\} \times \frac{f_+^2}{2\pi^3 M_K^2}, \qquad (A1)$$

where

$$A(E_\mu, E_\pi) = M_K (2 E_\mu E_\nu - M_K E'_\pi) + \frac{1}{4} m_\mu^2 E'_\pi = m_\mu^2 E_\nu$$

$$B(E_\mu, E_\pi) = m_\mu^2 (E_\nu - \tfrac{1}{2} E'_\pi)$$

$$C(E_\pi) = \tfrac{1}{4} m_\mu^2 E'_\pi .$$

Due to the bubble chamber geometry and other selection criteria mentioned, the detection efficiency of $K^+_{\mu 3}$ decay events is no longer a constant but is a function of E_μ and E_π. This detection-efficiency function $\mathcal{E}(E_\mu, E_\pi)$ is computed by the Monte Carlo method, which consists of randomly generating a total of about 35,000 hypothetical events (64 events from each of 560 decay origins) for each (E_μ, E_π) point. The 560 decay origins were obtained from a random sample of K^+ stopping points in the chamber. For a given value of ξ, the normalized, theoretical Dalitz-plot density function corrected for detection efficiency is then

$$W'(\xi, E_\mu, E_\pi) = \mathcal{N}(\xi) \cdot \rho(\xi, E_\mu, E_\pi) \cdot \mathcal{E}(E_\mu, E_\pi) \qquad \text{(A2)}$$

where $\mathcal{N}(\xi)$ is the normalization constant formed in such a way that

$$\int W(\xi, E_\mu, E_\pi)\, dE_\mu\, dE_\pi = N \text{ (total number of events)},$$

where the integration is over the area under consideration (in our case E_μ 145 → 195 and $E_\pi < 245$). To obtain the most likely value of ξ from experimental data, one can form the usual maximum-likelihood function,

$$L(\xi) = \prod_{\text{all exp. events}} W'(\xi, E_\mu, E_\pi). \qquad \text{(A3)}$$

To eliminate a possible μ bias, we modify the above procedure as follows. We divide the total region into 1-MeV intervals in μ^+ energy. Instead of $W(\xi, E_\mu, E_\pi)$, we introduce functions

$$V_n(\xi, E_\pi) = \mathcal{N}'_n(\xi)\, \rho[\xi, (E_\mu)_n, E_\pi]\, \mathcal{E}[(E_\mu)_n, E_\pi] \qquad \text{(A4)}$$

where $\mathcal{N}'_n(\xi)$ is the normalization constant formed in such a way that

$$\int V_n(\xi, E_\pi)\, dE_\pi = N_n.$$

(In our case $E_\pi < 245$ MeV.)

In Eq. (A4) N_n is the number of events in the nth bin. One then obtains the best value of ξ by forming the maximum-likelihood function

$$L(\xi) = \prod_n \left[\prod_{\substack{\text{all events} \\ \text{in nth bin}}} V_n(\xi, E_\pi) \right]. \tag{A5}$$

To obtain the theoretical expression for the μ^+ spectrum, one must integrate $\rho(\xi, E_\mu, E_\pi)$ in Eq. (A1) over pion energies. The result is[5]

$$W_2(\xi, E_\mu) \approx (E_\mu^2 - m_\mu^2)^{1/2} \frac{(\Delta - m_\pi^2 - 2 M_K E_\mu)^2}{(\Delta - 2 M_K E_\mu)} \left[D + F \operatorname{Re} \xi + G |\xi| \right]^2 \tag{A6}$$

where $\Delta = M_K^2 + m_\mu^2$

$$D = M_K E_\mu + \frac{1}{4} m_\mu^2 \left(\frac{M_K E_\mu - m_\mu^2}{\Delta - 2 M_K E_\mu} \right)$$

$$F = \frac{1}{2} m_\mu^2 \left(\frac{2 M_K^2 + m_\mu^2 - 3 M_K E_\mu}{\Delta - 2 M_K E_\mu} \right)$$

$$G = \frac{1}{4} m_\mu^2 \left(\frac{M_K E_\mu - m_\mu^2}{\Delta - 2 M_K E_\mu} \right).$$

B. Polarization of μ From $K^+_{\mu_3}$ Decay

Cabibbo and Maksymowicz[16] have shown that in $K^+_{\mu_3}$ decay the muon is completely polarized and its polarization direction is completely determined by $\underset{\sim}{p}_\mu$, $\underset{\sim}{p}_\pi$, and ξ. The μ polarization direction $\hat{P}_\mu$ can be expressed as

$$\hat{\underset{\sim}{P}}_\mu(\xi) = \frac{\underset{\sim}{A}(\xi)}{|\underset{\sim}{A}|(\xi)} \tag{A7}$$

$$\underset{\sim}{A}(\xi) = a_1(\xi)\, \underset{\sim}{p}_\mu - a_2(\xi) \left\{ \underset{\sim}{p}_\pi + \underset{\sim}{p}_\pi \left[\frac{(M_K - E_\pi)}{m_\mu} + \frac{(\underset{\sim}{p}_\pi \cdot \underset{\sim}{p}_\mu)(E_\mu - m_\mu)}{m_\mu |\underset{\sim}{p}_\mu|^2} \right] \right\}$$
$$+ (\operatorname{Im} \xi) \cdot M_K \cdot (\underset{\sim}{p}_\pi \times \underset{\sim}{p}_\mu), \tag{A8}$$

where

$$a_1(\xi) = \frac{M_K^2}{m_\mu} \left\{ 2 E_\nu + [\operatorname{Re}(\xi) - 1] \cdot E'_\pi \right\}$$

$$a_2(\xi) = M_K^2 + [\operatorname{Re}(\xi) - 1] M_K E_\mu + \frac{m_\mu^2}{4} \left\{ [\operatorname{Re}(\xi) - 1]^2 + [\operatorname{Im}(\xi)]^2 \right\}.$$

Note that the third term on the right side of Eq. (A8) gives rise to $P_\mu^\perp$, a polarization component normal to the decay production plane, and it is proportional to Im (ξ). Time-reversal invariance requires that Im (ξ) = 0, and thus also requires $P_\mu^\perp$ to vanish.

The asymmetry in the μ^+ decay is used to analyze the polarization of the μ^+. For a μ^+ polarized along the direction $\hat{P}_\mu$, the direction of the electron $\hat{p}_e$ path from the μ has a decay distribution

$$D = 1 + \alpha \hat{P}_\mu \cdot \hat{p}_e , \tag{A9}$$

where the asymmetry parameter α has a value $\alpha = 0.33$ averaged over all electron energies. If the magnetic-field direction is along $\hat{z}$, then the information obtainable is only on the component of $\underset{\sim}{P}_\mu$ along the z direction.

$$D' = 1 + \alpha(\hat{P}_\mu \cdot \hat{z})\ (\hat{z} \cdot \hat{p}_e). \tag{A10}$$

The maximum-likelihood function for the best value of ξ is then

$$L(\xi) = \prod_{\substack{\text{all} \\ \text{events}}} \{1 + \alpha[\hat{P}_\mu(\xi, \underset{\sim}{p}_\mu, \underset{\sim}{p}_\pi) \cdot \hat{z}](\hat{z} \cdot \hat{p}_e)\}. \tag{A11}$$

For the longitudinal polarization $\underset{\sim}{P}_\mu^\ell$, one forms a maximum-likelihood expression in exactly the same way as for the total μ polarization, except that the term $\hat{P}_\mu$ is replaced by $\underset{\sim}{P}_\mu^\ell = (\hat{P}_\mu \cdot \hat{p}_\mu)\,\hat{p}_\mu$ in Eq. (A11). For completeness, we give the other two components of the μ polarization:

$$\underset{\sim}{P}_\mu^\perp = (\hat{P}_\mu \cdot \hat{u})\,\hat{u}$$

$$\underset{\sim}{P}_\mu^T = (\hat{P}_\mu \cdot \hat{v})\,\hat{v},$$

where

$$\hat{u} = \frac{\hat{p}_\pi \times \hat{p}_\mu}{|\hat{p}_\pi \times \hat{p}_\mu|}$$

$$\hat{v} = \frac{\hat{u} \times \hat{p}_\mu}{|\hat{u} \times \hat{p}_\mu|}$$

C. K_{μ_3}/K_{e_3} Branching Ratio

The assumption of μ-e universality states that the expression for $K^+_{e_3}$ decay is the same as that for $K^+_{\mu_3}$ decay, except that the value of m_e is to replace m_μ in Eq. (A1). Furthermore, $f_\pm(\mu) = f_\pm(e)$. With these conditions we can integrate over the Dalitz density plot and obtain

$$R = [0.649 + 0.127 \text{ Re } \xi + 0.00193 |\xi|^2] \left| \frac{f_+(K_{\mu_3})}{f_+(K_{e_3})} \right|^2 . \qquad \text{(A12)}$$

If a value of ξ obtained from internal measurements on K_{μ_3} is used to predict R, the measurement of R thus provides a numerical test of μ-e universality in the form

$$\frac{f_+(K_{\mu_3})}{f_+(K_{e_3})} = \sqrt{R_{meas}/R_{pred}}$$

where R_{pred} is the expression in brackets in Eq. (A12) above.

Table I. Energy dependence of form factors.

λ^+	λ^-	Likelihood (arb. units)	Best value of Re ξ
-0.08	0	0.46	+2.30
-0.04	0	1.47	+1.42
0.00	0	2.42	+0.72
+0.04	0	1.58	+0.05
+0.08	0	0.41	-0.58
0	-0.40	2.07	-0.52
0	-0.20	2.31	-1.90
0	-0.10	2.19	+2.28
0	+0.10	2.27	+0.50
0	+0.20	1.59	+0.46
0	+0.40	2.20	+0.02

Table II. Summary of measurements of ξ.

Source	Experiment	Xi → ξ values
This experiment	μ^+ spectrum[a]	Re $\xi = 0.0^{+1.1}_{-0.9}$
		$\lvert\text{Im } \xi\rvert = 0.0 \pm 1.0$
	Muon longitudinal polarization ($P_\mu^{\parallel}$)[b]	Re $\xi = -0.7^{+0.9}_{-3.3}$
		$\lvert\text{Im } \xi\rvert = 0.5^{+1.4}_{-0.5}$
	$K^+_{\mu_3}/K^+_{e_3}$ branching ratio	For Im $\xi = 0$
		Re $\xi = +0.40 \pm 0.40$
		(or -6.98 ± 0.40)
	π^0 spectrum and	For Im $\xi = 0$
	π_μ angular correlation	Re $\xi = +0.72 \pm 0.37$
	Muon total polarization	Re $\xi = -1.4 \pm 1.8$
		Im $\xi = +1.6 \pm 1.3$
	Above experiments combined	Re $\xi = +0.34 \pm 0.24$
		Im $\xi = +0.69^{+0.57}_{-0.87}$
		For Im$\xi = 0$ / For complex ξ
V. Bisi et al.[c]	μ^+ spectrum and K_{μ_3} branching ratio	Re $\xi > -3.3$ / Re $\xi = -0.75 \pm 0.5$
		Re $\xi = +0.6 \pm 0.5$ (or -7.3 ± 0.5) / Im $\xi = +3.5 \pm 0.50$
G. Jensen et al.[d]	μ^+ and π^0 spectra and angular correlations	Re $\xi = -1.2 \pm 1.0$
		$0 \leq \lvert\text{Im } \xi\rvert \leq 2.4$ at 90% confidence level
G. Giacomelli et al.[e]	μ^+ spectrum	For Im $\xi = 0$
		Re $\xi = +0.7 \pm 0.5$
A. Boyarski et al.[f]	μ^+ spectrum	For Im $\xi = 0$
		Re $\xi = -7.6$ in best agreement with data
J. Brown et al.[g]	μ^+ and π^0 spectra and angular correlations	For Im $\xi = 0$
		Re $\xi = +1.8 \pm 1.6$
J. Dobbs et al.[h]	μ^+ spectrum	For Im $\xi = 0$
		Re $\xi = -9$ at 95% confidence level
D. Cutts et al.[i]	μ^+ spectrum and $P_\mu^{\parallel}$	For ξ complex
		$0.8 < \lvert\xi\rvert < 2.6$
V. Smirnitski and Weissenberg[j]	$P_\mu^{\parallel}$	For Im $\xi = 0$, Re $\xi = +2$
T. Groves et al.[k]	μ^- spectrum	For Im $\xi = 0$, Re $\xi = 0$
G. Borreani et al.[ℓ]	$P_\mu^{\parallel}$	For Im $\xi = 0$,
		Re $\xi = +1.2^{+2.4}_{-1.8}$

a. See Refs. 8 and 9.
b. See Ref. 2.
c. See Ref. 21.
d. See Ref. 16.
e. See Ref. 22.
f. See Ref. 23.
g. See Ref. 24.
h. See Ref. 25.
i. See Ref. 26.
j. See Ref. 27.
k. See Ref. 28.
ℓ. See Ref. 28.

FOOTNOTES AND REFERENCES

* Work done under the auspices of the U. S. Atomic Energy Commission.

† Present Address: Mississippi State University, Starkville, Mississippi.

‡ Present Address: Argonne National Laboratory, Argonne, Illinois.

1. U. Camerini, R. Hantman, R. March, D. Murphree, G. Gidal, G. Kalmus, W. Powell, R. Pu, C. Sandler, S. Natali, and M. Vallani, Phys. Rev. Letters 14, 989 (1965).
2. G. Gidal, W. Powell, R. March, and S. Natali, Phys. Rev. Letters 13, 95 (1964).
3. J. Brown, J. Kadyk, G. Trilling, R. Van de Walle, B. Roe and D. Sinclair, Phys. Rev. Letters 7, 423 (1961).
4. D. Luers, I. S. Mittra, W. J. Willis, and S. S. Yamamoto, Phys. Rev. 133, B1276 (1964); D. Luers, I. S. Mittra, W. J. Willis, and S. S. Yamamoto, Phys. Rev. Letters 7, 255 (1961).
5. N. Brene, L. Egardt, and B. Qvist, Nucl. Phys. 22, 553 (1961).
6. S. W. McDowell, Nuovo Cimento 6, 1445 (1957).
7. P. Dennery and H. Primakoff, Phys. Rev. 131, 1334 (1963), summarizes a number of specific models for the strangeness-changing current.
8. C. L. Sandler, Time Reversal, the Form Factor Ratio, and the Branching Ratio in $K^+_{\mu_3}$ Decay (Ph. D. Thesis), Lawrence Radiation Laboratory Report UCRL-16253, June 1965 (unpublished).
9. R. D. Hantman, Measurement of the μ^+ Spectrum From $K^+_{\mu_3}$ Decay (Ph. D. Thesis), University of Wisconsin, 1965 (unpublished).
10. N. Cabibbo, Nuovo Cimento 11, 837 (1959).
11. V. Bisi et al., Nuovo Cimento 25, 768 (1965).
12. L. Behr and P. Mittner, Nucl. Instr. Methods 20, 446 (1963).

13. G. E. Kalmus, A. Kernan, R. T. Pu, W. M. Powell, and R. Dowd, Phys. Rev. Letters 13, 3 (1964).

14. A. Callahan, R. March, and R. Stark, Phys. Rev. 146, B1436 (1965).

15. G. L. Jensen, C. T. Murphy, and B. P. Roe, Phys. Rev. 138, B1507 (1965) and references cited therein.

16. N. Cabibbo and A. Maksymowicz, Phys. Letters 9, 352 (1964); and erratum Phys. Letters 11, 360 (1964).

17. G. L. Jensen, F. S. Shaklee, B. P. Roe, and D. Sinclair, Phys. Rev. 135, B1431 (1964).

18. J. H. Christenson, J. W. Cronin, V. L. Fitch, and R. Turlay, Phys. Rev. Letters 13, 138 (1964).

19. N. Cabibbo, Phys. Letters 12, 137 (1965).

20. N. Cabibbo (Lawrence Radiation Laboratory), private communication, 1965.

21. V. Bisi, G. Borreani, R. Cester, A. De Benedetti, M. I. Ferrero, C. M. Garelli, A. Marzari-Chiesa, B. Quassiati, G. Rinaudo, M. Vigone, and A. E. Werbrouck, Phys. Rev. Letters 12, 490 (1964); and erratum, ibid. 12, 656 (1964); V. Bisi, G. Borreani, A. Marzari-Chiesa, G. Rinaudo, M. Vigone, and A. E. Werbrouck, Phys. Rev. 139, B1068 (1965).

22. G. Giacomelli, D. Monti, G. Quareni, A. Quareni-Vigudelli, W. Puschel, and J. Tietge, Nuovo Cimento 34, 6182 (1964).

23. A. M. Boyarski, E. C. Loh, L. Q. Niemela, D. M. Ritson, R. Weinstein, and S. Ozaki, Phys. Rev. 128, 2394 (1962).

24. J. L. Brown, J. A. Kadyk, G. H. Trilling, R. T. Van de Walle, B. P. Roe, and D. Sinclair, Phys. Rev. Letters 8, 450 (1962).

25. J. M. Dobbs, K. Lande, A. K. Mann, K. Reibel, F. J. Sciulli, H. Uto, D. H. White, and K. K. Young, Phys. Rev. Letters 8, 295 (1962).

26. D. Cutts, T. Elioff, and R. Stiening, Phys. Rev. 138, B969 (1965).

27. V. A. Smirnitski and A. O. Weissenberg, Phys. Rev. Letters 12, 223 (1964).

28. T. H. Groves, P. R. Klein, and V. Vanderburg, Phys. Rev. 135, B1269 (1964); JETP 48, 1604 (1965) [English trans. 21, 1078 (1965)].

29. G. Borreani, G. Gidal, G. Rinaudo, A. Werbrouck, A. Caforio, C. Garelli, S. Natali, and M. Villani, Phys. Rev. 140, B1686 (1965).

FIGURE CAPTIONS

Fig. 1. Photograph (left) of a typical $K^+_{\mu_3}$ event with both γ rays from the π^0 forming conversion pairs; tracks identified in the tracing at upper left.

Fig. 2. Probability that μ^+ will stop in the chamber, determined by Monte Carlo calculations, as a function of the μ^+'s kinetic energy. A, with fiducial and angular restrictions imposed in branching-ratio determination; B, with restrictions imposed in μ^+ spectrum determination; C, for μ^+ accompanied by a 90-MeV π^0 from which both γ rays convert.

Fig. 3. Distribution of π^0 momenta obtained by fitting converted γ rays from K_{π_2} decays to π^0 decays kinematics.

Fig. 4. Experimental μ^+ energy spectrum, after background was subtracted and corrections made for detection probability, with predictions from (a) vector($\xi \neq 0$), (b) scalar, and (d) tensor theories.

Fig. 5. Likelihood function from μ^+ spectrum events, represented by contours of constant likelihood in complex ξ plane. The large ex (X) denotes most probable point.

Fig. 6. Likelihood function from μ^+ longitudinal polarization determinations, represented by contours of constant likelihood in imaginary ξ plane. The large ex (X) denotes most probable point.

Fig. 7. T_μ vs T_π Dalitz plot showing observed and theoretical numbers of events in various regions.

Fig. 8. Likelihood function from π^0 spectrum determination at fixed μ^+ energies, represented by contours of constant likelihood in imaginary ξ plane.

Fig. 9. Likelihood function for energy dependence of form factor f_+, with f_+ assumed to equal $A\left[1 + \lambda + \frac{(q_k - q_\pi)^2}{m_\pi^2}\right]$.

Fig. 10. Experimental π^0 spectrum compared with predictions of vector($\xi = 0$, $\lambda = 0$), scalar, and tensor theories.

Fig. 11. Likelihood function from μ^+ total polarization determination, represented by contours of constant likelihood in imaginary ξ plane. The large ex (X) denotes most probable point.

Fig. 12. Combined likelihood function for all experiments (product of functions in Figs. 6, 7, 8, and 11). Curve of constant branching ratio corresponding to our experimental value is shown.

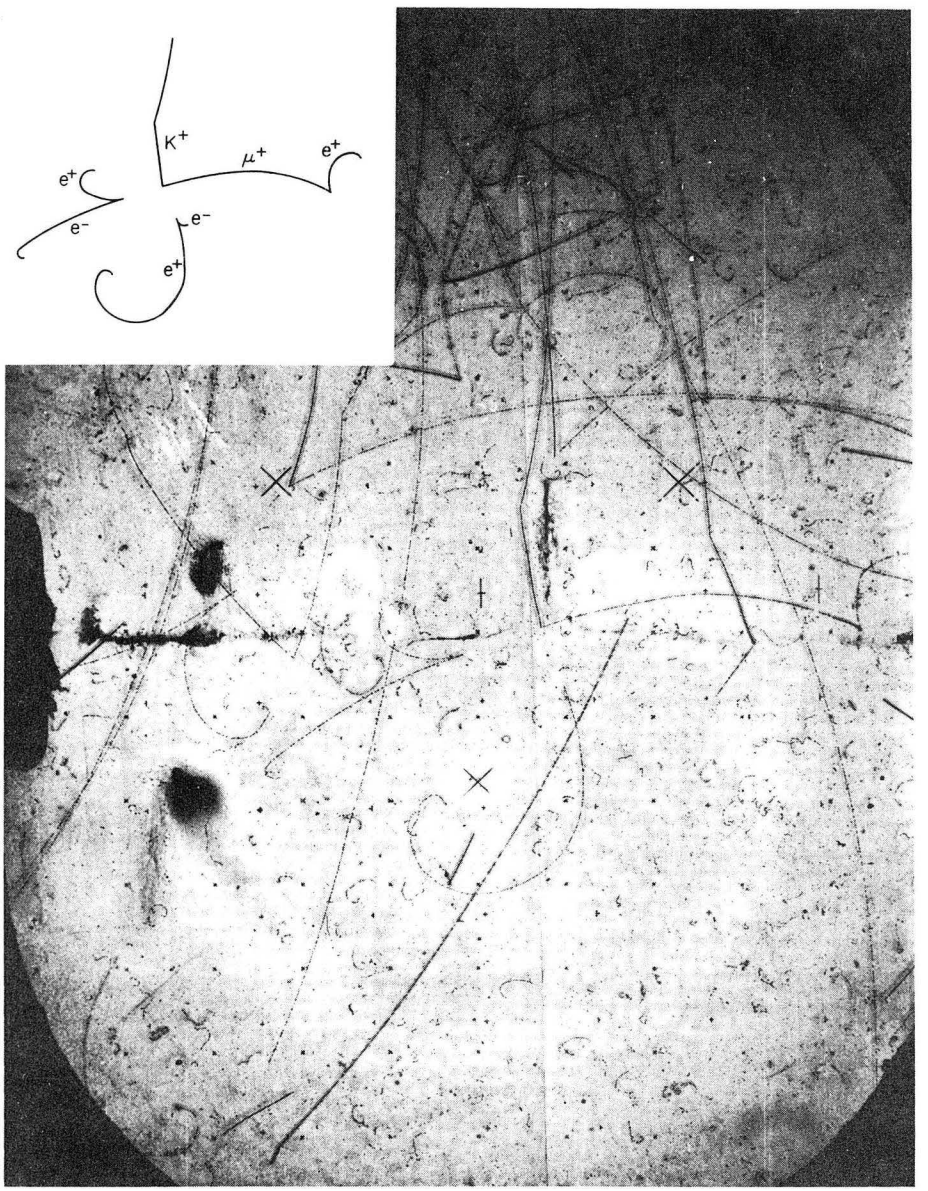

ZN-5389

Fig. 1

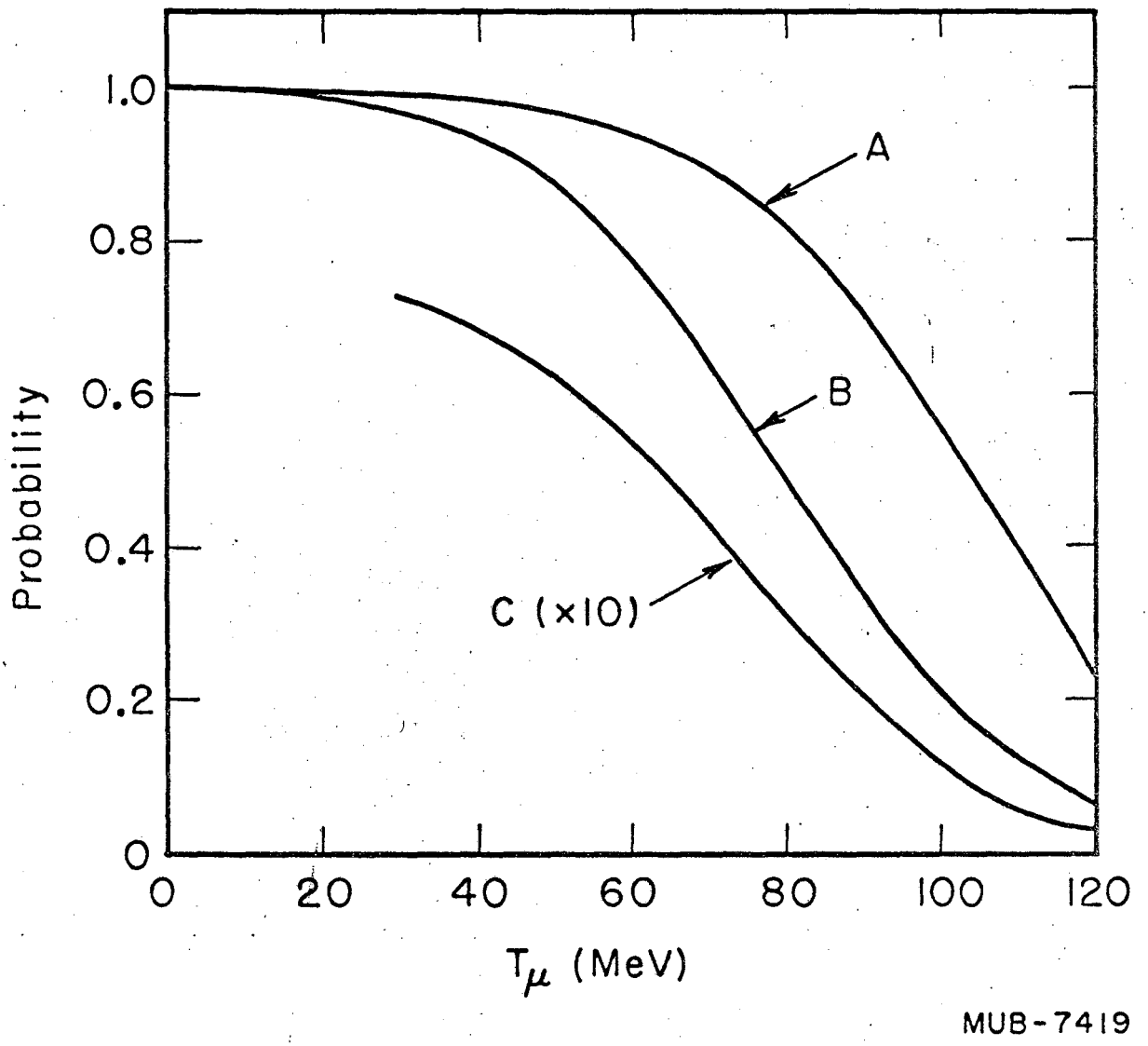
1.0
0.8
0.6
0.4
0.2
0
Probability
A
B
C (×10)
0
20
40
60
80
100
120
T_μ (MeV)
MUB-7419

Fig. 2

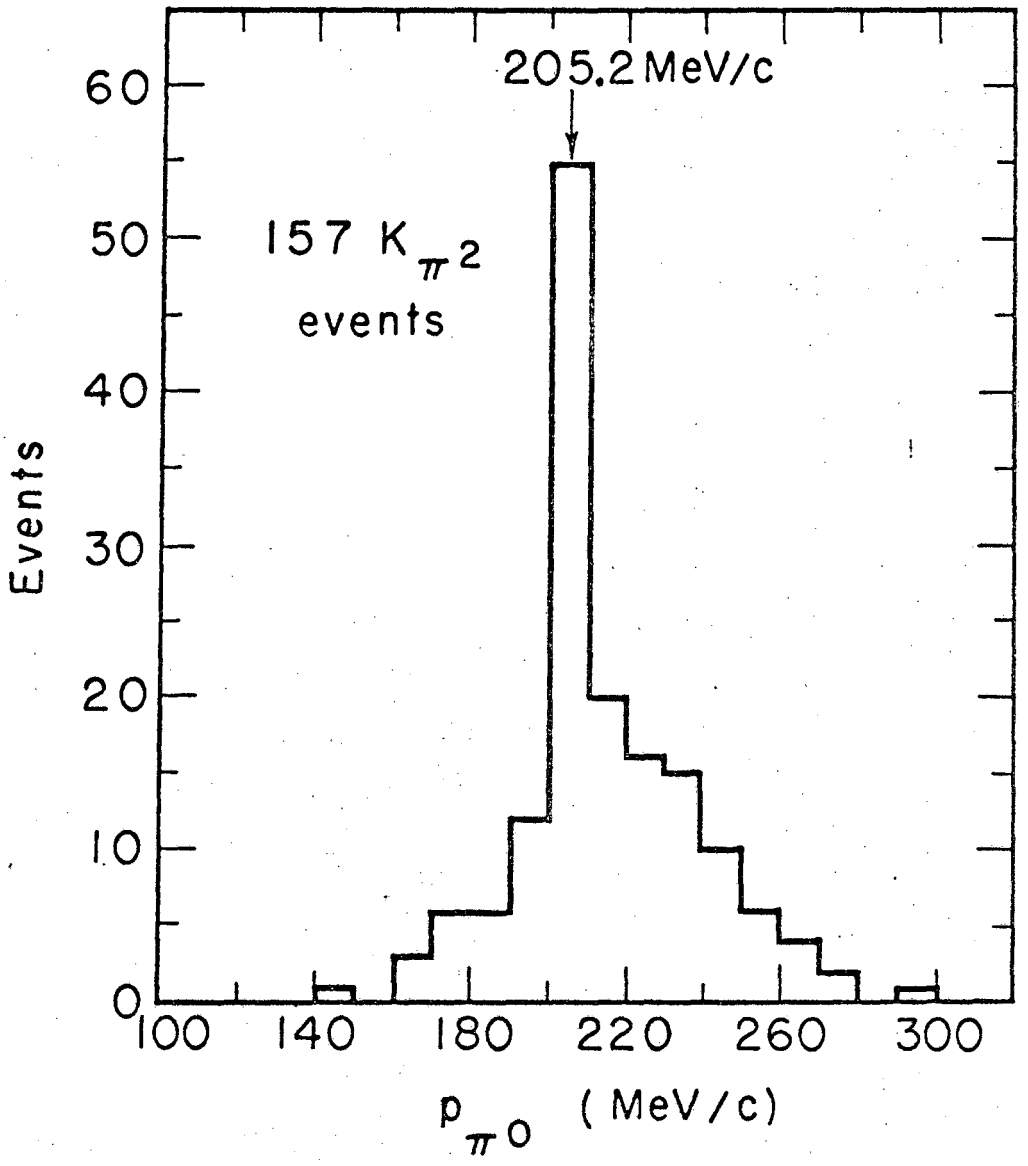

MUB-7418

Fig. 3

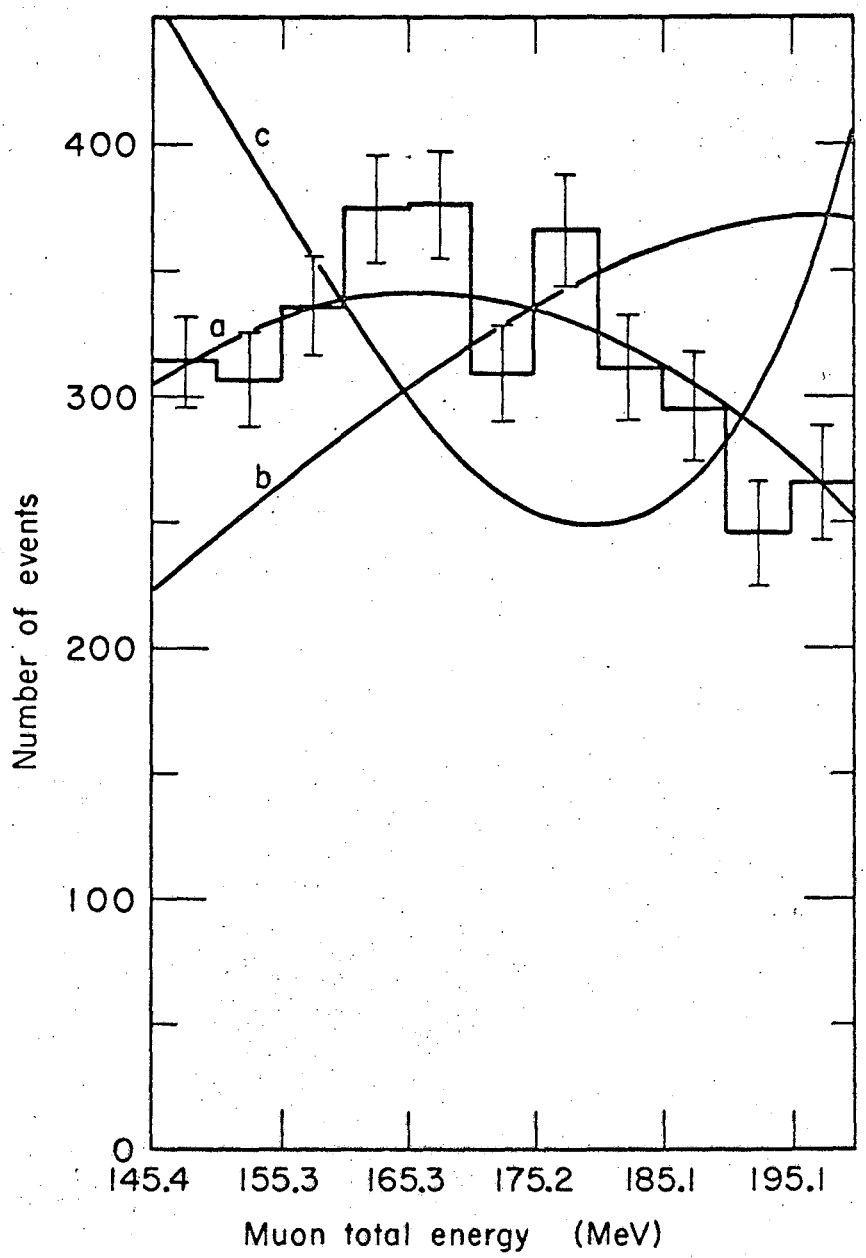
400
300
200
100
0
Number of events
a
b
c
145.4
155.3
165.3
175.2
185.1
195.1
Muon total energy (MeV)
MUB-9524

Fig. 4

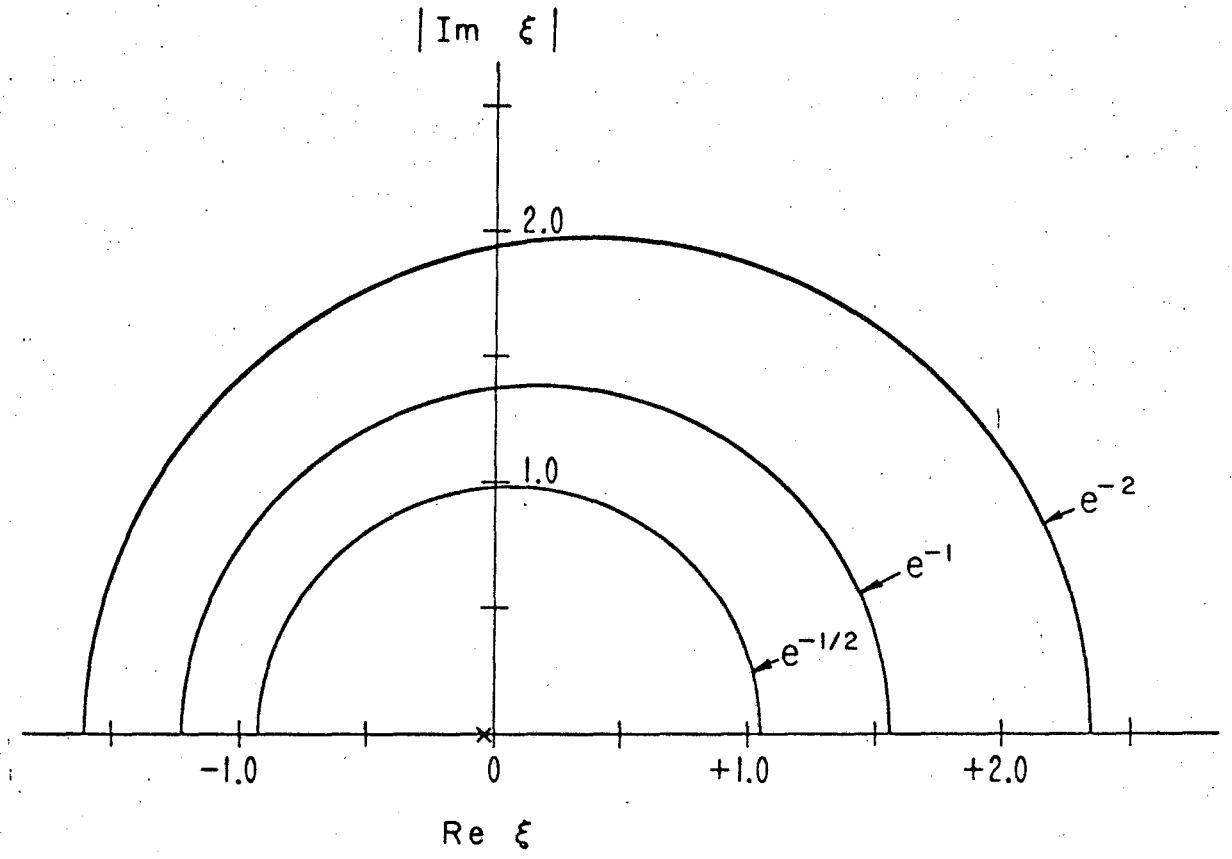

MUB-9243

Fig. 5

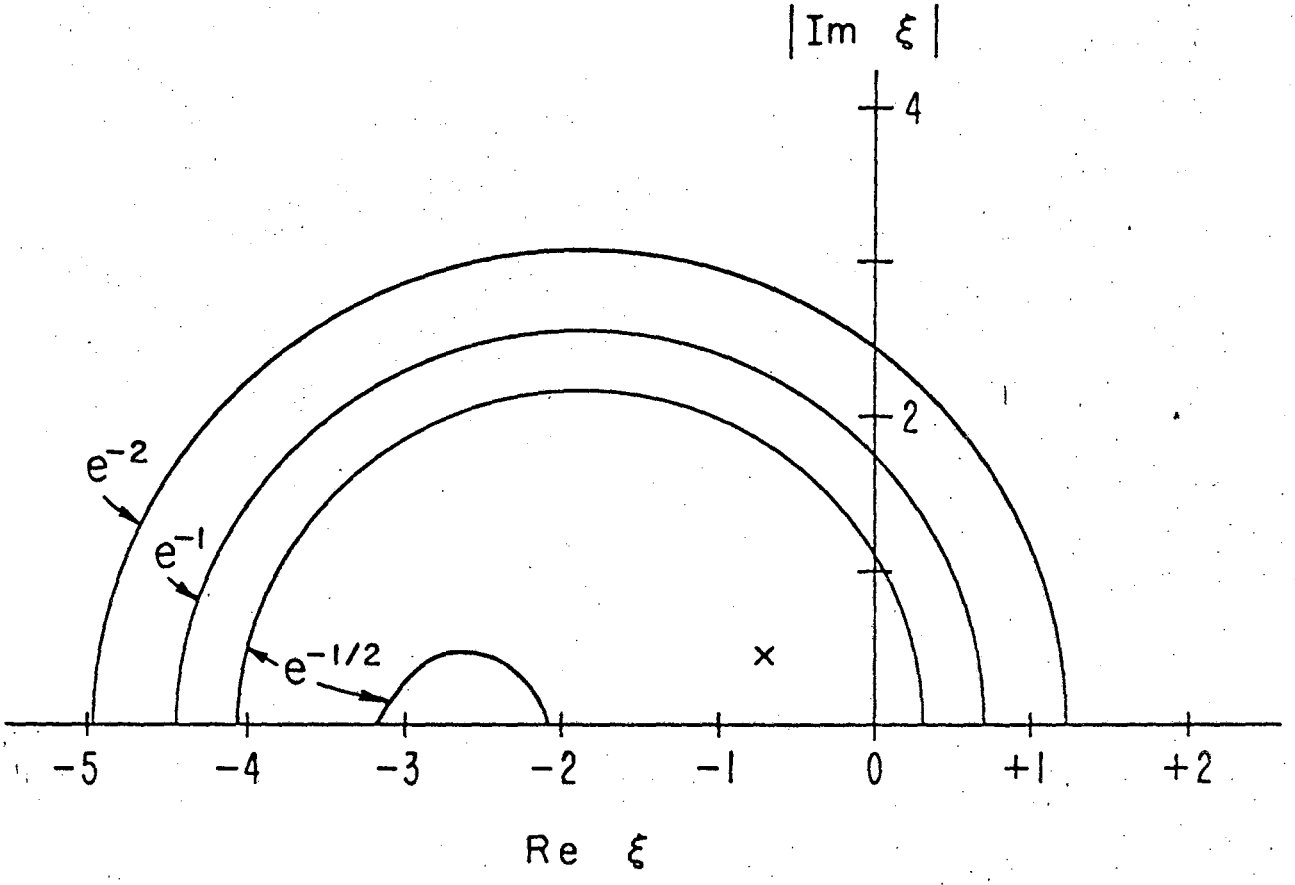

MUB-9242

Fig. 6

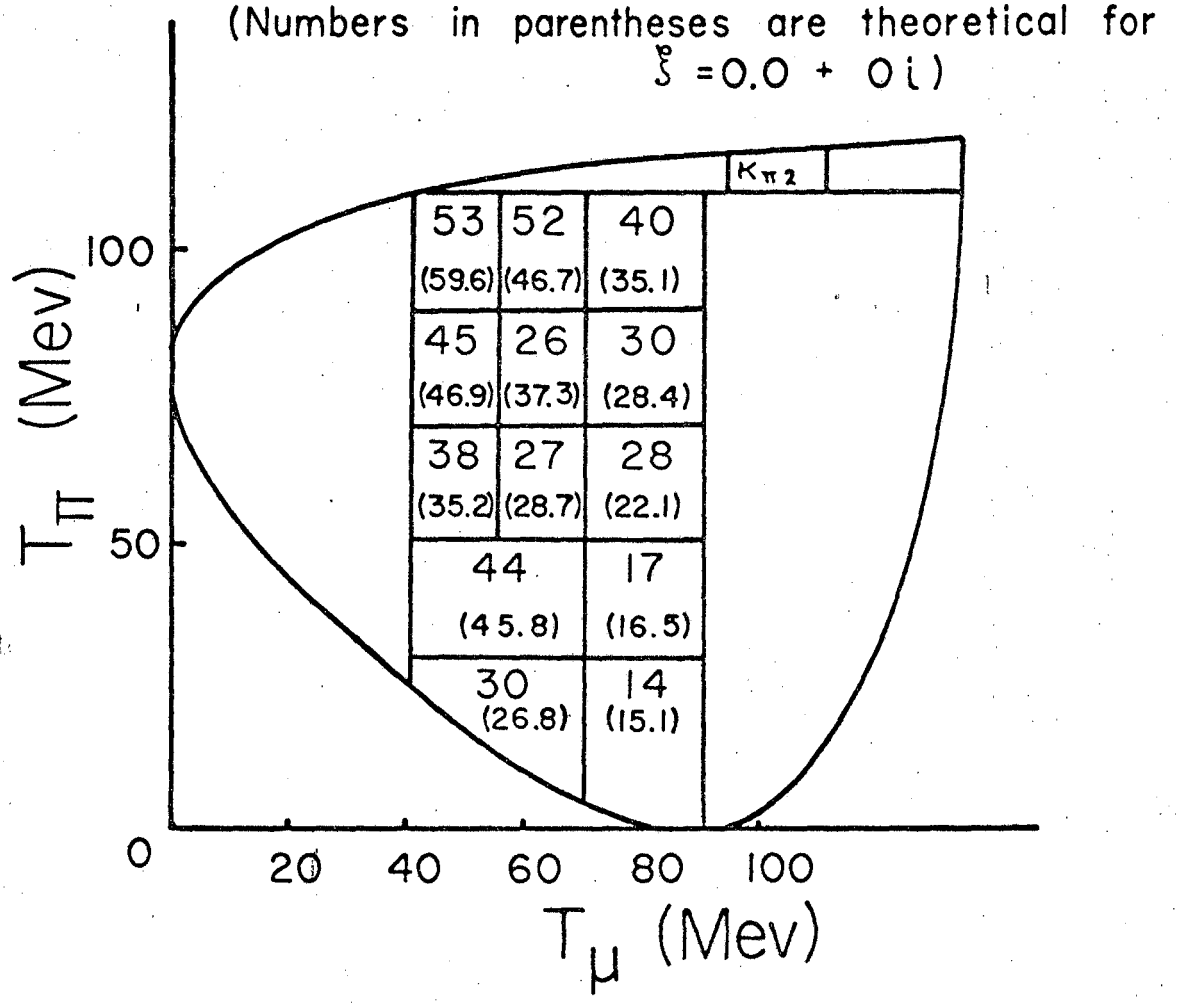

MUB-9342

Fig. 7

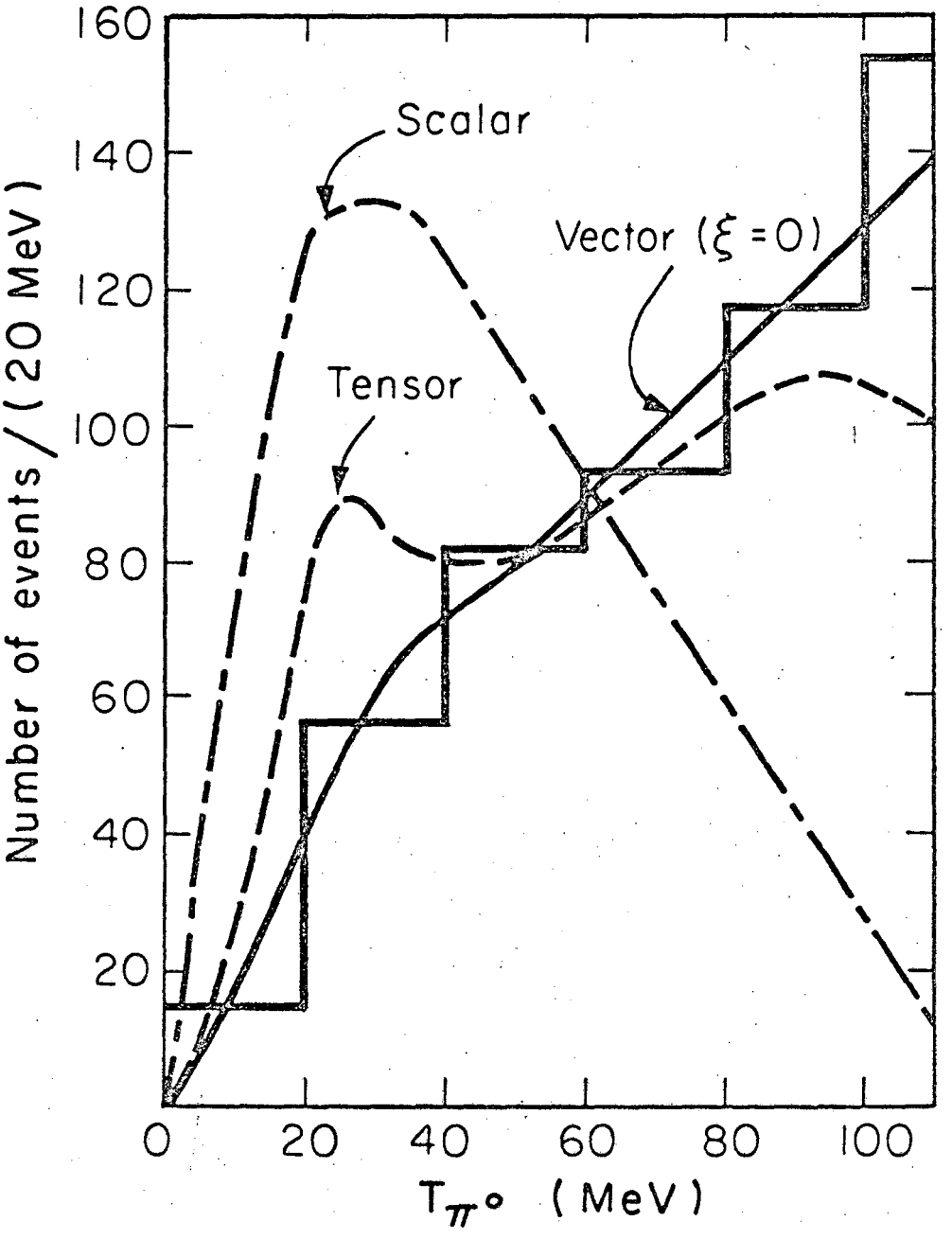
160
140
120
100
80
60
40
20
Number of events / (20 MeV)
Scalar
Vector (ξ = 0)
Tensor
0
20
40
60
80
100
Tπ° (MeV)
MUB-9251

Fig. 10

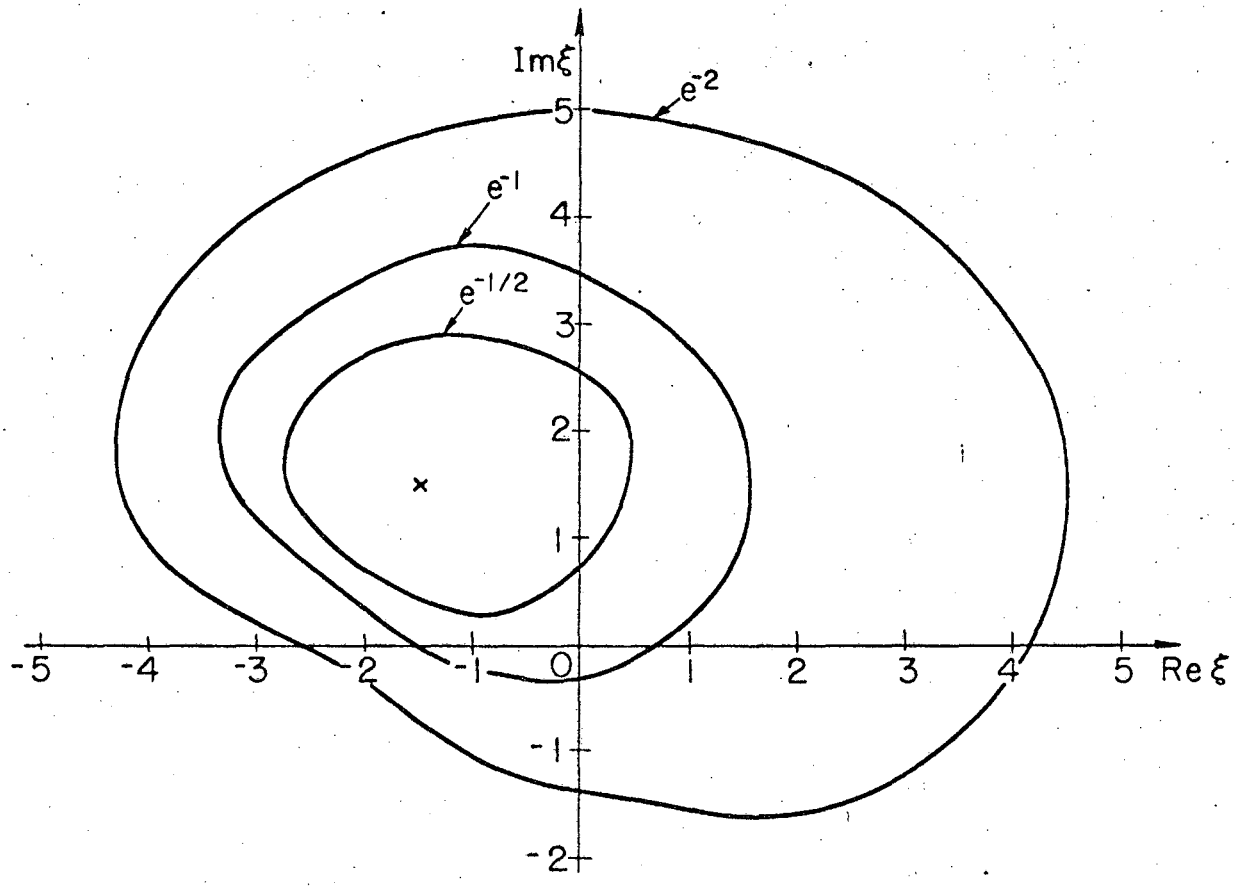

MUB-7423

Fig. 11

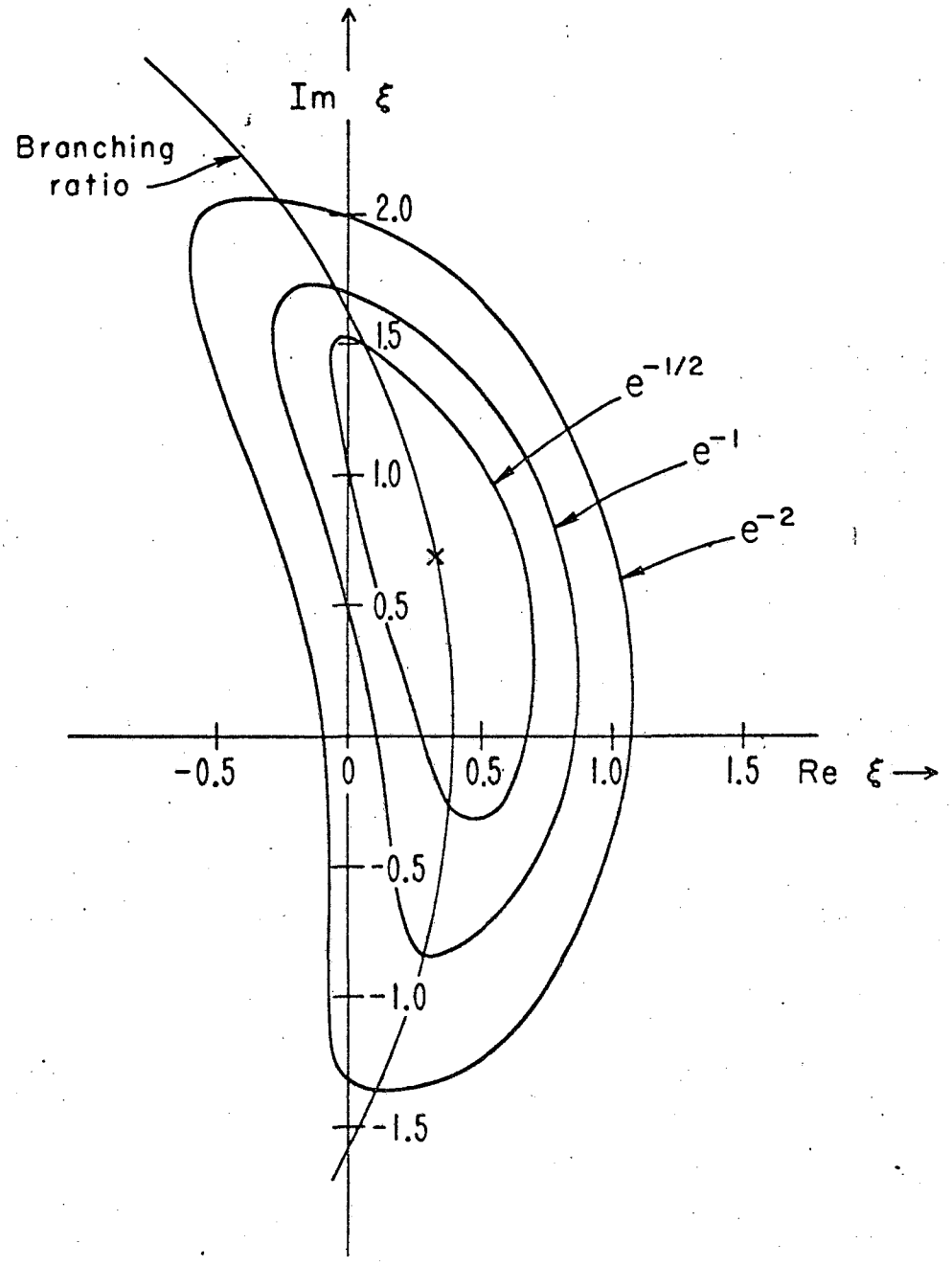
Im ξ
Branching ratio
2.0
1.5
1.0
0.5
-0.5
-1.0
-1.5
e^-1/2
e^-1
e^-2
-0.5
0
0.5
1.0
1.5
Re ξ
MUB-9244

Fig. 12